The Mixed-Valence Double-Cubanoid Cluster $[Fe_8S_{12}(Bu^tNC)_{12}]$: Synthesis, Structure, and Exchange Coupling of a New Structural Array of Four Fe(III) Sites

C. Goh,[†] A. Nivorozhkin,[†] S. J. Yoo,[‡] E. L. Bominaar,[‡] E. Münck,[‡] and R. H. Holm*,[†]

Department of Chemistry and Chemical Biology, Harvard University, Cambridge, Massachusetts 02138, and Department of Chemistry, Carnegie Mellon University, Pittsburgh, Pennsylvania 15213

Received January 26, 1998

Reaction of the cubane cluster $[Fe_4S_4(SEt)_2(Bu^tNC)_6]$ (**7**) and $PhCH_2SSSCH_2Ph$ in benzene solution affords the cluster $[Fe_8S_{12}(Bu^tNC)_{12}]$ (**6**) in 60−74% yield. The structure of this cluster as $[\mathbf{6}]\cdot 5C_6H_6$ and that of $[Fe_4S_4(SEt)_2(Bu^tNC)_6]$ (**8**, closely related to **7**) were determined by X-ray diffraction. Cluster **6** contains two cubanoid units $Fe_4S_5 = Fe_4(\mu_3\text{-}S)_3(\mu_3{:}\eta^2\eta^1\text{-}S_2)$ bridged by two μ_2-S ions and related by an inversion center. Certain features of the structure of **7** as revealed by **8** are retained in **6**, including in each cubanoid unit two low-spin distorted octahedral $Fe^{II}S_3(Bu^tNC)_3$ and two distorted tetrahedral $Fe^{III}(\mu_3\text{-}S)_3(\mu_2\text{-}S)$ sites and certain dimensional similarities. The formal insertion of an S(0) atom into a cubane to form a cubanoid unit disrupts one Fe−(μ_3-S) bond and leads to dimensional changes such as to poise one iron atom in a stereochemistry and position favorable for the formation of an Fe−(μ_2-S)−Fe bridge. The structures of iron−sulfur polycubanes are summarized; doubly sulfido-bridged double cubanes are unknown. In this family, cluster **6** is the only authenticated bis(μ_2-S) species and thus bears a distant relationship to the P clusters of nitrogenase. Cluster **6**, with four Fe(III) sites in the centrosymmetric array $[Fe_2(\mu_2\text{-}S)_2](\mu_2\text{-}S)_2$, presents an exchange coupling problem not previously encountered in iron−sulfur compounds. A formal treatment of the problem based on two coupling constants for intra- (J) and intercubanoid (J') exchange is presented. It is shown that the there is no unique solution for J,J'. Reasonable values of these parameters based on different assumptions are considered. If a recently determined J value for coupling in a $[Fe_2(\mu_2\text{-}S)_2]^{2+}$ fragment of a cubane cluster is adopted, $J = 280$ cm^{-1} and $J' = 445$ cm^{-1} for **6**.

Introduction

The imperative for the synthesis and investigation of polycubane iron−sulfur clusters, otherwise of considerable interest in their own right, derives from the structure of the P cluster of nitrogenase. This cluster has the Fe_8S_7 core composition and consists of cubane-type Fe_4S_4 and cuboidal Fe_4S_3 fragments joined by a common sulfur atom ($\mu_{5,6}$) and bridged by two cysteinate sulfur atoms.[1,2] Four cysteinate residues constitute the terminal ligands. The structure of the P cluster **1** is depicted in Figure 1 in the P^N oxidation state, in which the distance between a cuboidal iron atom and the central bridging sulfur atom is 2.9 Å (dashed line). This distance in the one-electron oxidized state P^{OX} is 3.9 Å, in which case the sulfur atom has the μ_5 bridging mode. Also shown in Figure 1 are the core structures of all known synthetic polycubane iron−sulfur clusters. These include the μ_2-S bridged double cubanes **2** with a variety of terminal ligands,[3−5] the rhomb-linked dicubane **3** with phosphine[6,7] and isonitrile[8] terminal ligands, the doubly bridged triple cubane **5**,[9] and the phosphine-ligated rhomb-linked tetracubane **4**.[7,10] The existence of **5** in solution was deduced from spectroscopic properties; structures of the other polycubanes have been established by X-ray diffraction.

A few years ago, we reported the synthesis of a new type of polynuclear iron−sulfur cluster composed of two Fe_4S_5 fragments bridged by two μ_2-S atoms.[6] The cluster $[Fe_8S_{12}(Bu^tNC)_{12}]$, shown as **6** in Figure 1, strictly speaking, is not a cubane cluster because of the composition of each fragment occasioned by the occurrence of a persulfide ligand. It is, however, sensibly considered with cubanes because it more closely resembles a cubane than any other known iron−sulfur cluster motif.[11] The descriptor "cubanoid" is perhaps appropriate. At the time of its report,[6] $[Fe_8S_{12}(Bu^tNC)_{12}]$ was obtainable only in minute yields ($\lesssim$3%); its structure was described, albeit very briefly. Since that time, we have developed a synthesis affording good yields, obtained crystals of improved diffraction quality, and investigated the Mössbauer spectroscopic and magnetic properties. $[Fe_8S_{12}(Bu^tNC)_{12}]$ is not intended as a P cluster model. However, it is the only cubane or cubanoid

[†] Harvard University.
[‡] Carnegie Mellon University.

(1) Peters, J. W.; Stowell, M. H. B.; Soltis, S. M.; Finnegan, M. G.; Johnson, M. K.; Rees, D. C. *Biochemistry* **1997**, *36*, 181. This structure supersedes earlier structural models of the P clusters deduced from X-ray data: Howard, J. B.; Rees, D. C. *Chem. Rev.* **1996**, *96*, 2965.
(2) Bolin, J. T.; Campobasso, N.; Muchmore, S. W.; Morgan, T. V.; Mortenson, L. E. In *Molybdenum Enzymes, Cofactors, and Model Systems*; Stiefel, E. I., Coucouvanis, D., Newton, W. E., Eds.; American Chemical Society: Washington, DC, 1993; pp 186−195.
(3) Challen, P. R.; Koo, S.-M.; Dunham, W. R.; Coucouvanis, D. *J. Am. Chem. Soc.* **1990**, *112*, 2455.
(4) Huang, J.; Mukerjee, S.; Segal, B. M.; Akashi, H.; Zhou, J.; Holm, R. H. *J. Am. Chem. Soc.* **1997**, *119*, 8662.
(5) Huang, J.; Holm, R. H. *Inorg. Chem.* **1998**, *37*, 2247.
(6) Cai, L.; Segal, B. M.; Long, J. R.; Scott, M. J.; Holm, R. H. *J. Am. Chem. Soc.* **1995**, *117*, 8863.
(7) Goh, C.; Segal, B. M.; Huang, J.; Long, J. R.; Holm, R. H. *J. Am. Chem. Soc.* **1996**, *118*, 11844.
(8) Harmjanz, M.; Saak, W.; Haase, D.; Pohl, S. *J. Chem. Soc., Chem. Commun.* **1997**, 951.
(9) Hoveyda, H. R.; Holm, R. H. *Inorg. Chem.* **1997**, *36*, 4571.
(10) While not directly pertinent to the present investigation, we note the existence of an extensive set of dicubanes containing MFe_3S_4 cores and bridged partly or entirely through the heterometal M: Huang, J.; Goh, C.; Holm, R. H. *Inorg. Chem.* **1997**, *36*, 356.
(11) For depictions of other structural motifs, see: Long, J. R.; Holm, R. H. *J. Am. Chem. Soc.* **1994**, *116*, 9987.

S0020-1669(98)00085-8 CCC: $15.00
Published on Web 06/15/1998

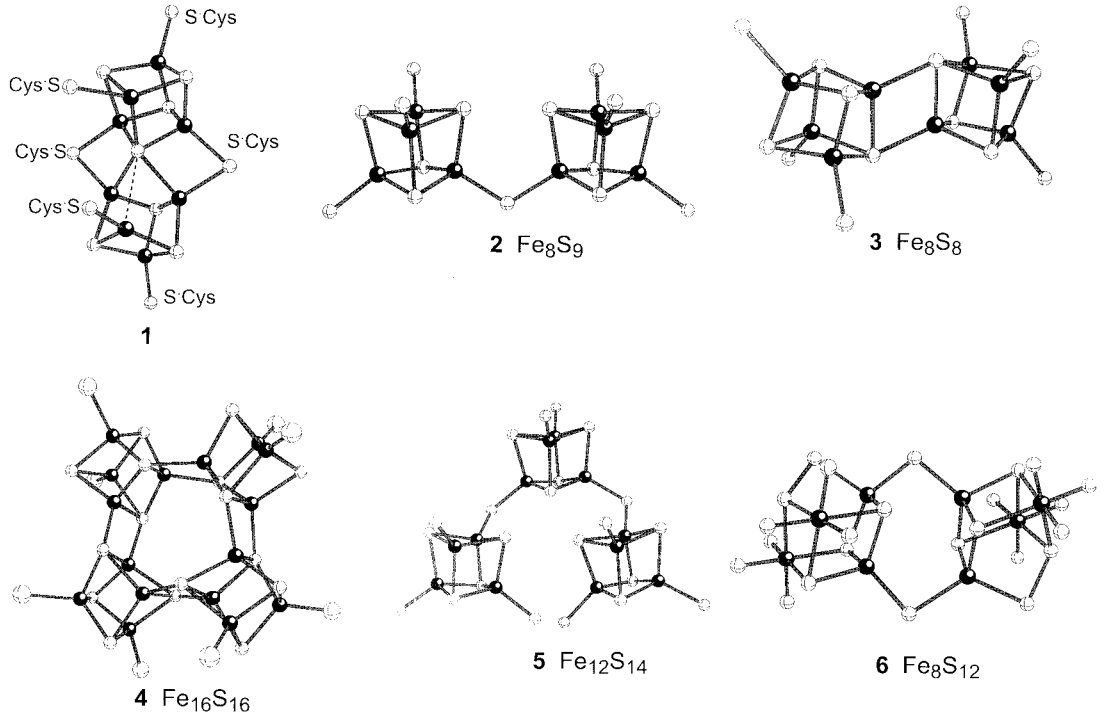

Figure 1. Schematic depictions of the structure of the P^N cluster of nitrogenase[1,2] (**1**) and the core units of all known iron−sulfur polycubanes (**2**−**6**).[3−9] Except for **5**,[9] all structures have been crystallographically established.

cluster bridged by two sulfur atoms; for this reason it is presently the closest synthetic approach to the P cluster. Because of its structure, $[Fe_8S_{12}(Bu^tNC)_{12}]$ presents an exchange coupling problem not previously encountered in iron−sulfur compounds. The results of our investigation of this cluster are described here. Clusters of principal interest are designated as indicated; compounds **7** and **8** have been previously reported.

$[Fe_8S_{12}(Bu^tNC)_{12}]$ **6**

$[Fe_4S_4(SEt)_2(Bu^tNC)_6]$ **7**[12]

$[Fe_4S_4(SBu^t)_2(Bu^tNC)_6]$ **8**[12]

Experimental Section

Preparation of $[Fe_8S_{12}(Bu^tNC)_{12}]$. All operations were performed under a pure dinitrogen atmosphere. A solution of 1.04 g (3.73 mmol) of dibenzyl trisulfide in 10 mL of benzene was added to a solution of 0.578 g (0.590 mmol) of $[Fe_4S_4(SEt)_2(Bu^tNC)_6]$[12] in 10 mL of benzene. The mixture was stirred for 1 h, filtered to remove a small amount of black residue, and allowed to stand for 5 days at ambient temperature. Large black crystals were collected by filtration, washed with benzene and ether, and dried in vacuo to afford 0.400 g (74%) of product. The procedure can be scaled up by a factor of 2 and has been repeated multiple times with yields in the range 60−74%. An analytical sample and that used for magnetic susceptibility measurements were recrystallized from acetonitrile/ether and dried in vacuo. Absorption spectrum (CH_2Cl_2): λ_{max} (ϵ_M) 345 (sh, 35 800), 425 (sh, 22 500), 565 (sh, 14 500) nm. IR (KBr): ν_{NC} 2130 (s), 2099 (sh), 2067 (sh) cm^{-1}. ^1H NMR ($CDCl_3$): δ 1.40 (1), 1.48 (1), 1.57 (1). Electrospray-MS: *m*/*z* 1828 (M^+). FAB-MS (3-nitrobenzyl alcohol): *m*/*z* 1828 (M^+), 1662 ($M^+ - 2L$), 1579 ($M^+ - 3L$), 1496 ($M^+ - 4L$), 1413 ($M^+ - 5L$), 1330 ($M^+ - 6L$), 1247 ($M^+ - 7L$) (L = Bu^tNC). Anal. Calcd for $C_{60}H_{108}Fe_8N_{12}S_{12}$: C, 39.40; H, 5.95; Fe, 24.43; N, 9.19; S, 21.03. Found: C, 40.02; H, 5.38; Fe, 24.41; N, 8.43; S, 21.22.

(12) Goh, C.; Weigel, J. A.; Holm, R. H. *Inorg. Chem.* **1994**, *33*, 4861.

Table 1. Crystallographic Data for $[Fe_4S_4(SBu^t)_2(Bu^tNC)_6]$ and $[Fe_8S_{12}(Bu^tNC)_{12}]\cdot 5C_6H_6$[a]

empirical formula	$C_{55}H_{96}Fe_4N_6S_6$	$C_{90}H_{138}Fe_8N_{12}S_{12}$
fw	1257.17	2219.68
cryst syst	monoclinic	monoclinic
space group	$P2_1/n$	$P2_1/c$
Z	4	2
a, Å	12.328(2)	15.1607(2)
b, Å	22.733(5)	20.1464(1)
c, Å	24.554(5)	21.3993(3)
β, deg	103.78(2)	109.902(1)
V, Å^3	6683(2)	6145.7(1)
T, K	223	213
d_{calc}, g/cm^3	1.185	1.094
μ, mm^{-1}	1.072	1.155
R,[b] wR_2[c]	0.0885, 0.2160	0.0912, 0.2435

[a] Graphite-monochromatized Mo Kα ($\lambda = 0.710\ 73$ Å). [b] $R = \sum||F_o| - |F_c||/|F_o|$. [c] w$R_2 = \{\sum[w(F_o^2 - F_c^2)^2]/\sum[w(F_o^2)^2]\}^{1/2}$.

X-ray Structure Determination. Diffraction-quality crystals of [**8**]·$2C_6H_6$·C_5H_{12} and [**6**]·$5C_6H_6$ were isolated from vapor diffusion of pentane into a benzene solution and from the initial crystallization of the benzene reaction mixture, respectively. Data were collected on a Nicolet P3 ([**8**]·$2C_6H_6$·C_5H_{12}) or a Siemens SMART ([**6**]·$5C_6H_6$) diffractometer. Crystal parameters are given in Table 1. Crystals showed no significant decay during the data collections. The raw intensity data were converted (including corrections for scan speed, background, Lorentz, and polarization effects) to structure factor amplitudes and their esd's. Empirical absorption corrections based on observed variations in azimuthal (ψ) scans were applied. The structures were solved by direct methods and were refined by full-matrix least-squares and Fourier techniques. The asymmetric unit of [**8**]·$2C_6H_6$·C_5H_{12} consists of one cluster, two benzene solvate molecules, and one pentane solvate molecule. The asymmetric unit of [**6**]·$5C_6H_6$ contains one-half of the cluster, two benzene solvate molecules, and one-half benzene solvate molecule disordered across an inversion center. Thermal parameters for all non-hydrogen atoms in the clusters were refined anisotropically. In the final stages of refinement, hydrogen atoms were assigned to ideal positions and refined using a rigid model with isotropic thermal parameters 1.5 times that of the attached carbon atom. In the last cycle of refinement, all parameters shifted by <1%

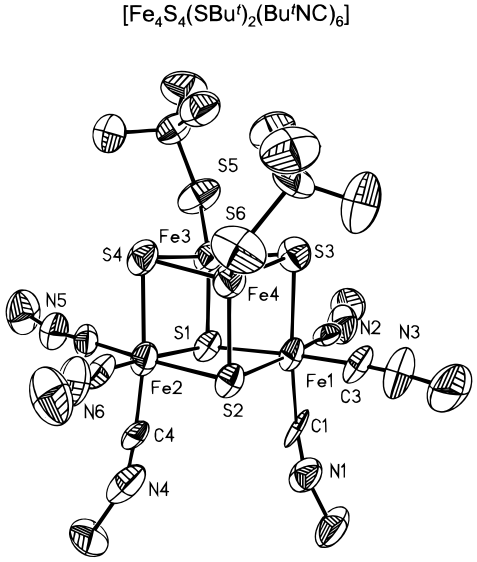

Figure 2. Structure of $[Fe_4S_4(SBu^t)_2(Bu^tNC)_6]$ (**8**) as its bis(benzene)·pentane solvate, showing 50% probability ellipsoids and the atom labeling scheme. For clarity, the methyl groups of the isonitrile ligands are omitted and not all coordinated carbon atoms are labeled.

of their esd's, and final difference Fourier maps showed no significant electron density. Final R-factors are given in Table 1.[13]

Other Physical Measurements. Mössbauer spectra were obtained using a constant-acceleration spectrometer. Isomer shifts are quoted relative to iron metal at 298 K. Magnetic susceptibility measurements were carried out with a MPMS SQUID susceptometer from Quantum Design.

Results and Discussion

Synthesis. Clusters of the type $[Fe_4S_4L_2(Bu^tNC)_6]$ ($L = Cl^-$, ArO^-, RS^-), such as **8** in Figure 2, have a cubane-type structure containing two octahedral low-spin $Fe^{II}S_3(Bu^tNC)_3$ sites and two tetrahedral $Fe^{III}S_3L$ sites. They undergo regiospecific substitution at the tetrahedral sites with displacement of L.[12,14] Our intention was to produce sulfide-bridged polycubanes using the regiospecific substitution property of this cluster type, which includes $[Fe_4S_4(SEt)_2(Bu^tNC)_6]$.[12] Originally, **6** was discovered as a product formed in slight yield by the reaction of **7** with H_2S.[6] Subsequently, dibenzyl trisulfide was found to be a far more effective sulfur source in a system with the apparent stoichiometry of reaction 1. One such system, with initial mol

$$2[Fe_4S_4(SEt)_2(Bu^tNC)_6] + 4(PhCH_2)_2S_3 \rightarrow [Fe_8S_{12}(Bu^tNC)_{12}] + 2EtSSEt + 4PhCH_2SSCH_2Ph \quad (1)$$

ratio $(PhCH_2)_2S_3$:**7** = 6:1 in benzene at ambient temperature, was monitored by ^1H NMR. The thiolate signals of **7** at 4.97 (CH_3) and 37.5 (CH_2) ppm slowly disappeared, and resonances from the product trisulfides appeared together with others apparently due to symmetric and asymmetric di- and trisulfides. Weak paramagnetically shifted resonances of unidentified cluster species were also observed. The two *tert*-butyl signals of **7** near 1.3 ppm were supplanted by two or three new resonances centered about 1.4 ppm. While we have no information on what must be a complex reaction pathway, the mean iron oxidation state ($Fe^{2.5+}$) is unchanged between reactant and product. The formation of **6** requires two equivalents of sulfide. These must arise from the reduction of a S(0) species, presumably by ethanethiolate, and are incorporated as bridging atoms. In addition, 1 equiv of S(0), probably arising largely from the initial trisulfide, is inserted into each starting cluster. After several days, the black crystalline product appearing in the NMR tube was identified by FAB-MS and ^1H NMR as **6**. The three *tert*-butyl resonances observed in chloroform solution near 1.5 ppm and of about equal intensity are consistent with the C_{2h} symmetry of the cluster in the solid state (vide infra).

When the reaction was conducted multiple times on a preparative scale, the cluster product was isolated after 2−4 days as block-shaped black crystals in yields of 60−74%. Reactions of the clusters $[Fe_4S_4L_2(Bu^tNC)_6]$ ($L = Cl^-$, ArO^-)[12,14] with potential bridging reagents such as $(Me_3Si)_2S$, Na_2S, and Li_2S afforded intractable and/or unidentified cluster products. Reaction 1 remains the method of choice for the synthesis of **6**.

Table 2. Selected Interatomic Distances (Å) and Angles (deg) for $[Fe_4S_4(SBu^t)_2(Bu^tNC)_6]$

Fe(II) Sites			
Fe(1)−S(1)	2.350(4)	Fe(2)−S(1)	2.348(4)
Fe(1)−S(2)	2.332(4)	Fe(2)−S(2)	2.334(4)
Fe(1)−S(3)	2.368(5)	Fe(3)−S(4)	2.373(5)
Fe(1)−Fe(2)	3.444(3)		
Fe(1)−Fe(3)	3.043(3)	Fe(2)−Fe(3)	3.025(3)
Fe(1)−Fe(4)	3.033(4)	Fe(2)−Fe(4)	3.038(5)
Fe(1,2)−C(1−6)	range 1.81(2)−1.88(2), mean 1.85(2)		
S−Fe(1,2)−S	range 84.8(1)−94.5(1)		
S−Fe(1,2)−C	range 85.7(4)−90.4(4), mean 88(2)		
C−Fe(1,2)−C	range 88.6(6)−100.3(6)		
Fe(III) Sites			
Fe(3)−S(1)	2.239(4)	Fe(4)−S(2)	2.248(4)
Fe(3)−S(3)	2.248(4)	Fe(4)−S(4)	2.252(4)
Fe(3)−S(4)	2.249(4)	Fe(4)−S(3)	2.248(4)
mean of 6	2.247(4)		
Fe(3)−Fe(4)	2.758(3)		
Fe(3)−S(5)	2.254(5)	Fe(4)−S(6)	2.263(5)
S(3)−Fe(3)−S(4)	102.5(2)	S(3)−Fe(4)−S(4)	102.4(2)
Fe(3)−S(3)−Fe(4)	75.7(1)	Fe(3)−S(4)−Fe(4)	75.6(1)

Structures. (a) $[Fe_4S_4(SBu^t)_2(Bu^tNC)_6]$. As will be seen, product cluster **6** retains certain structural features of precursor cluster **7**. Because the X-ray structure of **7** has not yet been obtained, we utilize for comparison that of the closely related cluster **8** shown in Figure 2. Because structural features of $[Fe_4S_4L_2(Bu^tNC)_6]$ clusters are similar and have been discussed,[12,14] an abbreviated list of metric features is provided in Table 2. The $[Fe_4S_4]^{2+}$ core faces of **8** consist of nonplanar rhombs. For later reference, the mean deviations from the least-squares planes Fe(1,2)S(1,2) and Fe(3,4)S(3,4) are 0.076 and 0.143 Å, respectively, and the dihedral angle between the planes is 0.2°. Cluster **8** contains two distorted octahedral, low-spin $Fe^{II}S_3(Bu^tNC)_3$ sites Fe(1,2) and two distorted tetrahedral $Fe^{III}S_4$ sites Fe(3,4) which closely approach C_{3v} symmetry. There is no imposed symmetry on the molecule. Because of the long Fe(1)−Fe(2) separation (3.444(3) Å) and the shorter Fe(3)−Fe(4) distance (2.758(3) Å), the $[Fe_4S_4]^{2+}$ core is truncated such that the smaller face contains Fe(3,4). The additional long Fe(1,2)−Fe(3,4) distances (mean 3.035(8) Å) ensure no significant metal−metal bonding interactions involving Fe(1,2). The dimensions of the rhomb Fe(3,4)S(3,4) approach those of $[Fe_2S_2(SR)_4]^{2-}$ complexes.[15] Like the latter species, **7** (and by

(13) See paragraph at the end of this article for Supporting Information available.

(14) Weigel, J. A.; Srivastava, K. K. P.; Day, E. P.; Münck, E.; Holm, R. H. *J. Am. Chem. Soc.* **1990**, *112*, 8015.

(15) (a) Mayerle, J. J.; Denmark, S. E.; DePamphilis, B. V.; Ibers, J. A.; Holm, R. H. *J. Am. Chem. Soc.* **1975**, *97*, 1032. (b) Cai, J.; Cheng, C. *Jiegou Huaxue* (*J. Struct. Chem.*) **1988**, *7*, 43. (c) Ueyama, N.; Ueno, S.; Sugawara, T.; Tatsumi, K.; Nakamura, A.; Yasuoka, N. *J. Chem. Soc., Dalton Trans.* **1991**, 2723.

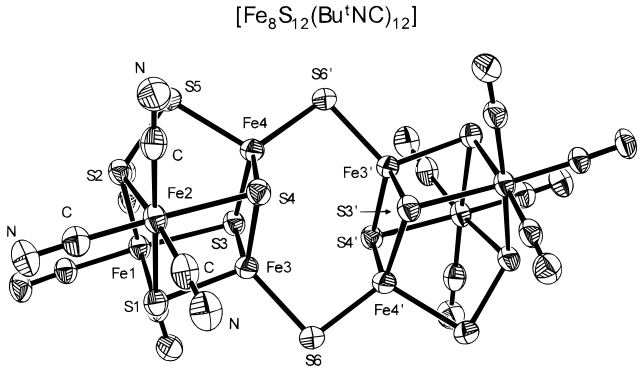

Figure 3. Structure of $[Fe_8S_{12}(Bu^tNC)_{12}]$ (**6**) as its pentakis(benzene) solvate, showing 50% probability ellipsoids and the atom labeling scheme. Primed and unprimed atoms are related by a symmetry center. For clarity, *tert*-butyl groups are omitted and the carbon and nitrogen atoms on only one iron atom are indicated.

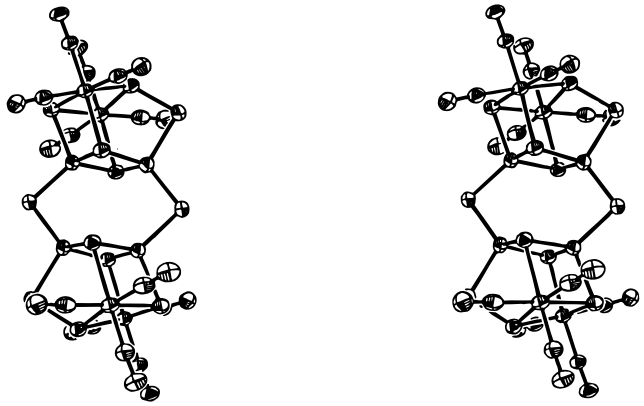

Figure 4. Stereoview of the structure of $[Fe_8S_{12}(Bu^tNC)_{12}]$ presented in the orientation of Figure 3.

inference, **8**) is antiferromagnetically coupled with an $S = 0$ ground state.[16]

(b) $[Fe_8S_{12}(Bu^tNC)_{12}]$.[17] The compound **[6]**·$5C_6H_6$ crystallizes readily from the benzene reaction solution. The structure of the cluster is presented in Figure 3, and a stereoview is provided in Figure 4. Selected metric data are set out in Table 3. As is seen, the cluster contains two Fe_4S_5 fragments that are coupled through two μ_2-S atoms and related by an inversion center. The nearly planar rhomb Fe(3,4)S(3,4) and that related by symmetry are parallel and separated by the nonbonded distances Fe(3)···Fe(4′) = 3.285(2) Å and S(3)···S(4′) = 3.454(2) Å. An idealized mirror plane bisects the Fe(3,4)S(3,4) and Fe(1,2)S(1,2) core faces and is coincident with the plane containing Fe(3)S(6)Fe(4′), Fe(3′)S(6′)Fe(4), and the core disulfide S(2)−S(5).

The principal difference between the Fe_4S_5 fragment and the $[Fe_4S_4]^{2+}$ core of **8** is insertion of one S(0) atom, nominally into the Fe(4)−S(2) bond of a cubane core (Figure 3). Clusters containing the cubanoid Fe_4S_5 core are well established.[18−20] Of the two known forms of this core type, $Fe_4(\mu_3\text{-}S)_3(\mu_3{:}\eta^2\eta^2\text{-}S_2)$[17] (**9a**) and $Fe_4(\mu_3\text{-}S)_3(\mu_3{:}\eta^2\eta^1\text{-}S_2)$[18] (**9b**), the latter connectivity applies to **6**. Each fragment includes two low-spin

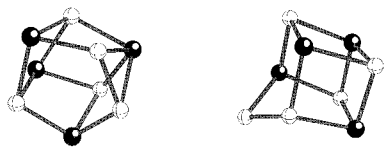

9a **9b**

Table 3. Selected Interatomic Distances (Å) and Angles (deg) for $[Fe_8S_{12}(Bu^tNC)_{12}]$

	Fe(II) Sites		
Fe(1)−S(1)	2.364(2)	Fe(2)−S(1)	2.369(2)
Fe(1)−S(2)	2.342(2)	Fe(2)−S(2)	2.343(2)
Fe(1)−S(3)	2.392(4)	Fe(2)−S(4)	2.390(2)
Fe(1)−Fe(2)	3.494(2)		
Fe(1)−Fe(3)	3.021(4)	Fe(2)−Fe(3)	3.033(4)
Fe(1)−Fe(4)	3.656(3)	Fe(2)−Fe(4)	3.646(3)
Fe(1,2)−C(1−6)	range 1.827(7)−1.873(8), mean 1.85(1)		
Fe(1,2)−C−N	range 173.1(7)−178.0(7), mean 176(2)		
C−Fe(1,2)−C	range 88.8(3)−98.8(3), mean 94(4)		
S(1)−Fe(1)−S(2)	83.24(7)	S(1)−Fe(2)−S(2)	83.10(6)
S(1)−Fe(1)−S(3)	95.81(6)	S(1)−Fe(2)−S(4)	96.18(6)
S(2)−Fe(1)−S(3)	95.86(6)	S(2)−Fe(2)−S(4)	96.13(7)
Fe(1)−S(1)−Fe(2)	95.18(7)	Fe(1)−S(2)−Fe(2)	96.46(7)
Fe(1)−S(2)−S(5)	111.94(9)	Fe(2)−S(2)−S(5)	111.97(9)
	Fe(III) Sites		
Fe(3)−S(1)	2.259(5)	Fe(4)−S(3)	2.277(2)
Fe(3)−S(3)	2.257(2)	Fe(4)−S(4)	2.274(2)
Fe(3)−S(4)	2.260(2)		
mean of 5	2.265(9)		
Fe(3)−S(6)	2.216(2)	Fe(4)−S(6′)	2.194(2)
Fe(4)−S(5)	2.289(2)	Fe(4)−S(2)	3.154(3)
Fe(3)−Fe(4)	2.798(1)	Fe(3)−Fe(4′)	3.285(2)
S(3)−Fe(3)−S(4)	104.19(7)	S(3)−Fe(4)−S(4)	103.10(7)
Fe(3)−S(3)−Fe(4)	76.18(6)	Fe(3)−S(4)−Fe(4)	76.20(6)
Fe(3)−S(1)−Fe(1)	80.75(6)	Fe(1)−S(3)−Fe(4)	103.05(7)
Fe(3)−S(3)−Fe(1)	80.17(6)	Fe(2)−S(4)−Fe(4)	102.83(7)
Fe(3)−S(1)−Fe(2)	80.30(6)	S(3)−Fe(4)−S(4)	103.10(7)
Fe(3)−S(4)−Fe(2)	79.85(6)	S(3)−Fe(4)−S(5)	104.38(7)
S(1)−Fe(3)−S(3)	102.75(7)	S(4)−Fe(4)−S(5)	104.77(8)
S(1)−Fe(3)−S(4)	103.20(7)	S(4)−Fe(4)−S(6′)	115.48(8)
S(3)−Fe(3)−S(4)	104.19(7)	S(3)−Fe(4)−S(6′)	115.15(8)
S(1)−Fe(3)−S(6)	111.34(7)	S(5)−Fe(4)−S(6′)	112.68(7)
S(3)−Fe(3)−S(6)	117.38(8)		
S(4)−Fe(3)−S(6)	116.23(8)		
Fe(3)−S(6)−Fe(4′)	96.29(7)		
S(2)−S(5)	2.104(2)	S(3)−S(4′)	3.454(2)
Fe(4)−S(5)−S(2)	91.67(8)		

sites $Fe^{II}(1,2)$ (vide infra) with distorted octahedral FeS_3C_3 coordination units having bond distances and angles closely comparable with the Fe(1,2) sites of **8**. The persulfide ligand S(2,5) bridges atoms Fe(1,2,4); its bond length of 2.104(2) Å is very close to that in Na_2S_2 (2.13 Å)[21] and comparable with other bridging persulfides.[22] The S(2) atom is part of the Fe(1,2)S(1,2) rhomb face of the core. Although S(2) is μ_2-bridging and part of the disulfide, only minor changes are found for its bond lengths and angles compared to the bonding of μ_3-S atoms in **8**. For example, the mean Fe(1,2)−S(2) distance of 2.343 Å compares well with the mean of 2.35(2) Å for the six Fe(1,2)−(μ_3-S) bonds in **8** and with mean of 2.367 Å for the Fe(1,2)−S(1) bonds in **6**. Similarly, the mean of the angles S(1)−

(16) Yoo, S. J.; Hu, Z.; Goh, C.; Bominaar, E. L.; Holm, R. H.; Münck, E. *J. Am. Chem. Soc.* **1997**, *119*, 8732.
(17) Crystal and molecular parameters determined previously[6] and in this work (at 223 and 213 K, respectively) are in good agreement. Data from the more recent determination are to be preferred.
(18) (a) Kubas, G. J.; Vergamini, P. J. *Inorg. Chem.* **1981**, *20*, 2667. (b) Jordanov, J.; Gaillard, J.; Prudon, M. K.; van der Linden, J. G. M. *Inorg. Chem.* **1987**, *26*, 2202.
(19) (a) $[Cp_4Fe_4S_5]^{1+}$: Dupré, N.; Auric, P.; Hendriks, H. M. J.; Jordanov, J. *Inorg. Chem.* **1986**, *25*, 139. (b) $(MeCp)_4Fe_4S_5]^{1+}$: Blonk, H. L.; Mesman, J.; van der Linden, J. G. M.; Steggerda, J. J.; Smits, J. M. M.; Beurskens, G.; Beurskens, P. T.; Tonon, C.; Jordanov, J. *Inorg. Chem.* **1992**, *31*, 962.
(20) (a) $[Cp_4Fe_4S_5]^{2+}$: Dupré, N.; Hendriks, H. M. J.; Jordanov, J.; Gaillard, J.; Auric, P. *Organometallics* **1984**, *3*, 800. (b) $[(Me_5Cp)_3Fe_4S_5(S_2C_2Ph_2)]^{0,+,2+}$: Inomata, S.; Tobita, H.; Ogino, H. *Inorg. Chem.* **1992**, *31*, 722. Inomata, S.; Hitomi, K.; Tobita, H.; Ogino, H. *Inorg. Chim. Acta* **1994**, *225*, 229.

Fe(1,2)−S(2) (83.17°) in **6** is quite close to the corresponding value (84.8°) in **8**. Other comparisons can be made with the data in Tables 2 and 3.

The bridges formed in **6** are Fe(4)−S(6′)−Fe(3′) and its symmetry-related counterpart. Each of the FeS_4 coordination units has distorted tetrahedral (C_{3v}) stereochemistry. The bonds to S(6) (0.04 Å) and S(6′) (0.09 Å) are shorter by the indicated amounts than the Fe−S bonds within the fragment, which for each site are nearly equal. The principal structural effect of persulfide ligation in cluster **6** is to position atom Fe(4) such that a bridge can be formed. Clearly the Fe(4)···S(2) separation of 3.154(3) Å (compared to 2.259(5) Å for Fe(3)−S(1)) modifies a distance and bonding constraint present in cubane cores. The core face Fe(1,2)S(1,2) has a mean deviation from its least-squares plane of 0.110 Å. The opposite face Fe(3,4)S(3,4) approaches planarity, with a mean deviation of 0.042 Å. Unlike the parallel alignment of opposite faces in **8**, the two planes of **6** define a dihedral angle of 18.7° Further, Fe(4) deviates from the plane Fe(3)S(3,4) by 0.171 Å and Fe(3) from the plane Fe(4)S(3,4) by 0.168 Å. These two planes form a dihedral angle of 6.9°. The dihedral angles and atom displacements from planes, together with the absence of an Fe(4)−S(2) bond, are such as to dispose Fe(3,4) toward the opposite fragment to an extent that sustains stable bridge bonds. The Fe(4)−S(6′) bridge bond length of 2.194(2) Å is indistinguishable from the bridge bond in $\{[Fe_4S_4Cl_3]_2(\mu_2\text{-}S)\}^{4-}$ (**2**, 2.206(4) Å).[2] The Fe(4)−S(6′)−Fe(3′) bridge angle of 96.29(7)° compares rather closely to the corresponding value in **2** (102.2°). Because this bond in **2** suffers no obvious constraint from the double-cubane structure, we conclude that any strain in the bridge bonds in **6** is not clearly evident, especially in their distance.

It should be noted that the double-cubane **2** (Figure 1) contains one sulfide bridge and that there are no authenticated clusters that contain two such bridges. In a recent study of the self-condensation reactions of the functionalized cluster $[Fe_4S_4(SH)_4]^{2-}$, we found no evidence for the formation of a doubly bridged double cubane. Instead, the doubly bridged tricubane **5** was deduced to be the principal polycubane product.[9] A small set of doubly bridged $MoFe_3S_4$ double cubanes containing one Fe−S−Fe bridge is known.[23] The other bridge, as well as one bridge in the only proven bis(μ_2-S) double-cubane,[23a] involves an octahedral molybdenum site. It appears probable that the double cubane core $Fe_8S_{10} = [Fe_4S_4]_2(\mu_2\text{-}S)_2$ with bridge dimensions similar to those in **6** is of marginal stability owing to stereochemical constraints at the putative bridging iron sites and attendant repulsion between bridged core faces. Attempts to prepare such a species by removal of S(0) from **6** with tertiary phosphines have not succeeded.

The clusters $[Fe_4S_4L_2(Bu^tNC)_6]$ (L = Cl^-, ArO^-, RS^-) exhibit chemically reversible one-electron oxidation and reduction over a potential interval of *ca*. 1.2 V.[12,14] The double-cubanoid cluster **6** behaves analogously. As shown by the cyclic voltammogram in Figure 5, two reductions and two oxidations are observed over a range of 1.9 V in acetonitrile. Controlled potential coulometry at +0.2 V confirmed $n = 2.0$ e for the two oxidations. Comparable diffusion currents indicate that the reductions are also one-electron processes. These oxidations must occur at the Fe(II) sites. Unfortunately, species formed by the oxidation of **6** with $[Cp_2Fe](BF_4)$ in acetonitrile have proven insufficiently stable for isolation.

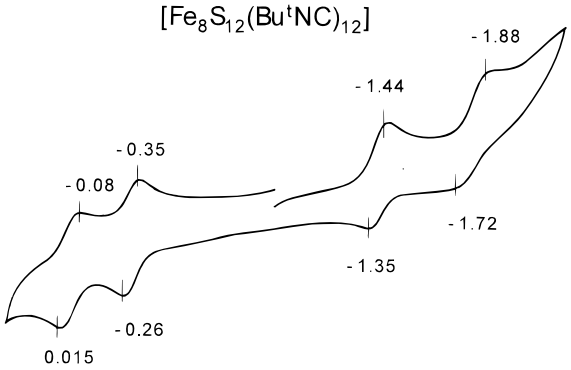

Figure 5. Cyclic voltammogram (100 mV/s) of $[Fe_8S_{12}(Bu^tNC)_{12}]$ in acetonitrile solution; peak potentials vs SCE are indicated.

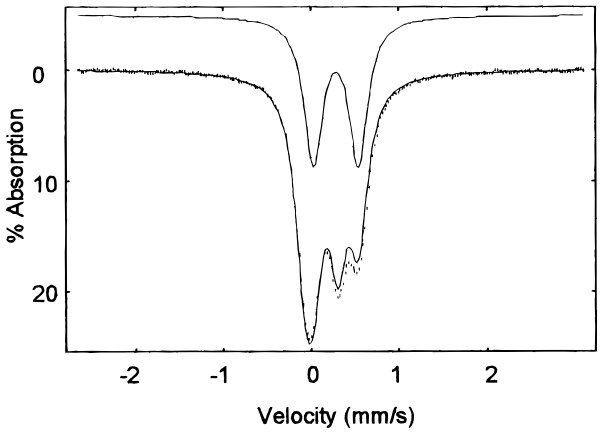

Figure 6. Mössbauer spectrum of $[Fe_8S_{12}(Bu^tNC)_{12}]$ recorded at 4.2 K in zero magnetic field. The solid line through the data is a theoretical fit using the parameters given in the text; the doublet shown above the data is the spectrum of the $Fe^{III}S_4$ sites.

Mössbauer Spectroscopy and Magnetism. Shown in Figure 6 is a 4.2-K Mössbauer spectrum of a polycrystalline sample of **6**; the sample measured was taken from the same batch as that used for the susceptibility studies described below. The spectrum consists of two quadrupole doublets whose low-energy lines overlap. Because the isomer shifts of high-spin $Fe^{III}S_4$ sites ($\delta = 0.25-0.30$ mm/s) and low-spin $Fe^{II}S_3(Bu^tNC)_3$ sites ($\delta < 0.2$ mm/s) differ, the two doublets, each representing four equivalent iron sites, are readily recognized. The solid line drawn through the data of Figure 6 is a least-squares fit to two doublets with $\Delta E_Q = 0.38$ mm/s and $\delta = 0.11$ mm/s for the low-spin ferrous sites and $\Delta E_Q = 0.57$ mm/s and $\delta = 0.28$ mm/s for the high-spin ferric sites of **6**; full width at half-maximum for all lines was 0.25 mm/s. Shown separately above the data is the doublet assigned to the $Fe^{III}S_4$ sites. Spectra recorded at 4.2 K in an 8.0-T applied field (not shown) indicate that the ground state of **6** is diamagnetic. Moreover, the Mössbauer spectra do not reveal any iron other than that attributed to **6**; possible iron impurities must be less than 3% of total iron. Parameters of the low-spin sites are consistent with those for related clusters, including **7** and **8**.[12,14]

The magnetic system of double-cubanoid cluster **6** consists of two symmetry-related rhombs ((Fe(3,4)S(3,4), Fe(3′,4′)S(3′,4′)) bridged by two sulfide atoms (S(6,6′)). Exchange interactions are expected among pairs of Fe(III) sites in the same

(21) Föppl, H.; Busmann, E.; Frorath, F. K. *Z. Anorg. Allg. Chem.* **1962**, *314*, 12.
(22) (a) Müller, A.; Jaegermann, W. *Inorg. Chem.* **1979**, *18*, 2631. (b) Müller, A.; Jaegermann, W.; Enemark, J. H. *Coord. Chem. Rev.* **1982**, *46*, 245.
(23) (a) Coucouvanis, D.; Challen, P. R.; Koo, S.-M.; Davis, W. M.; Butler, W.; Dunham, W. R. *Inorg. Chem.* **1989**, *28*, 4181. (b) Challen, P. R.; Koo, S.-M.; Kim, C. G.; Dunham, W. R.; Coucouvanis, D. *J. Am. Chem. Soc.* **1990**, *112*, 8606. (c) Demadis, K. D.; Chen, S.-J.; Coucouvanis, D. *Polyhedron* **1994**, *13*, 3147.

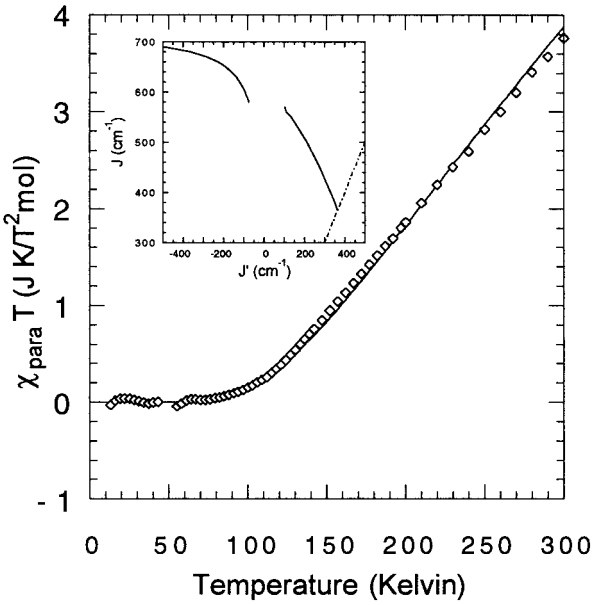

Figure 7. Plot of $\chi_{para}T$ vs T for $[Fe_8S_{12}(Bu^tNC)_{12}]$ in a field of 1 tesla. The solid curve is a representative fit of the data. Inset: solutions for J and J' from fitting the data in the figure with eqs 2 and 3. The broken line indicates points where $J = J'$.

and in different Fe_4S_5 fragments. We are unaware of any array of four paramagnetic iron sites resembling this structural arrangement.

Presented in Figure 7 is a plot of $\chi_{para}T$ vs T in the temperature range 10−300 K. The paramagnetic susceptibility of the cluster, χ_{para}, was extracted from the raw data following the procedure described elsewhere.[16] The data for χ_{para}T have been fitted with eq 2,

$$\chi_{para}T = \frac{g^2\mu_B^2 N}{3k}\frac{\sum_{S,\alpha}(2S+1)S(S+1)\exp(-E_{S,\alpha}/kT)}{\sum_{S,\alpha}(2S+1)\exp(-E_{S,\alpha}/kT)} \quad (2)$$

where N is the Avogadro number, k the Boltzmann constant, and μ_B the Bohr magneton. The sum in eq 2 runs over the energy eigenvalues ($E_{S,\alpha}$) of the system. S is the total spin ($S = \Sigma_{i=1}^{4} S_i$), and α labels different states with the same spin. As we are essentially dealing with a tetranuclear spin system with local spins $S_i = {}^5/_2$ (the spins of the Fe(II) sites being zero), there is generally more than one spin multiplet for each value of the total spin. The recurrence numbers are given by 6(0), 15(1), 21(2), 24(3), 24(4), 21(5), 15(6), 10(7), 6(8), 3(9), 1(10), where the values of S are indicated in parentheses. The energies $E_{S,\alpha}$ are obtained by diagonalization of the spin Hamiltonian (eq 3). In adopting eq 3, it is assumed that the "nonbridging"

$$H = J(S_1\cdot S_2 + S_3\cdot S_4) + J'(S_1\cdot S_4 + S_2\cdot S_3) \quad (3)$$

interactions vanish. In diagram **10** where iron atoms (1,3) and

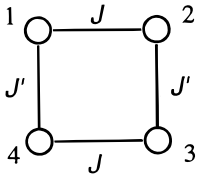

10

(2,4) are in different cubanoid fragments, $J_{13} = J_{24} = 0$. The relations $J_{12} = J_{34} = J$ and $J_{14} = J_{23} = J'$ follow from the symmetry of the cluster. The energy eigenvalues are invariant under interchange of J and J'. As a consequence, analysis of the susceptibility data does not allow a definite assignment of the fit values for J and J' to the parameters for intracubanoid and intercubanoid exchange. The computational procedure adopted in the evaluation of the eigenvalues takes advantage of the fact that an isotropic exchange Hamiltonian, such as eq 3, does not mix states with different total spin. For this reason, the diagonalization can be carried out separately for each allowed value of S. Thus, this procedure involves the construction and diagonalization of symmetric ($n \times n$) matrixes, where the dimensions (n) are the aforementioned recurrence numbers. While the Hamiltonian matrix for $J(S_1\cdot S_2 + S_3\cdot S_4)$ is diagonal in the pair-coupled basis $|(S_{12},S_{34})S\rangle$ ($S_{ij} = S_i + S_j$), the term $J'(S_1\cdot S_4 + S_2\cdot S_3)$ has also off-diagonal elements in this basis. The Hamiltonian matrix of the latter operator was obtained by a unitary transformation of its diagonal representation in the $|(S_{14},S_{23})S\rangle$ basis, and the transformation matrixes, $\langle(S_{14},S_{23})S|(S_{12},S_{34})S\rangle$, were expressed in terms of Racah coefficients by repeated spin recoupling. The Hamiltonian matrixes for the individual pair interactions ($J_{ij}S_i\cdot S_j$) need to be calculated only once and stored for multiple use in calculations with variable exchange parameters.

The solid curve in Figure 7 is the best fit resulting from minimization with respect to J and J' of the root-mean-squares sum of the deviations between theoretical (eq 2) and experimental values for $\chi_{para}T$. The analysis reveals that there is no unique solution for J and J'; the data in Figure 7 can be fitted with a family of correlated exchange parameters which is given by the curve in Figure 7 (inset). The curve, consisting of two branches, has been constructed by minimization of the root-mean-square deviation with respect to J', taking the value for J fixed. The fits associated with the points on this curve are of good quality, though the simulations slightly deteriorate near the gap between the two branches. Redundant solutions with $J < J'$ (i.e., those below the line $J = J'$) have not been indicated in the figure. The general solutions on the two branches bear the essential features of those at the extremes. At one extreme ($J = J' = 364$ cm^{-1}), the Hamiltonian can be written as eq 4, where c is a constant independent of S. The eigenfunctions of

$$H = c + {}^1/_2 J[S^2 - S_{13}{}^2 - S_{24}{}^2] \quad (4)$$

the Hamiltonian in eq 4 are given by the coupled spin functions $|(S_{13},S_{24})S\rangle$, and the corresponding energy eigenvalues are expressed by eq 5. For $J > 0$, the ground state is $|(5,5)0\rangle$ (S_{13}

$$E(S_{13},S_{24},S) = c + {}^1/_2 J[S(S+1) - S_{13}(S_{13}+1) - S_{24}(S_{24}+1)] \quad (5)$$

$= S_{24} = {}^5/_2 + {}^5/_2 = 5$), while the first and second excited states are $|(5,5)1\rangle$ and $|(5,5)2\rangle$. Excited states with $S_{13} < 5$ (or $S_{24} < 5$) are much higher in energy and do not significantly contribute to the susceptibility. For example, the state $|(4,5)1\rangle$ is separated by energy $E(4,5,1) - E(5,5,0) = 6J \approx 2200$ cm^{-1} from the ground state, leading to small Boltzmann factors, e.g., 2×10^{-5} at room temperature. Thus, the spin dependence of the relevant exchange energies of the four-iron set is given by the expression for the exchange energy of a dimer, ${}^1/_2 JS(S+1)$. At the other extreme (outside Figure 7, inset), J' is $-\infty$ and J asymptotically approaches 728 cm^{-1}. In this limit, the spins S_1 and S_4 (and S_2 and S_3) are coupled to resultant spin $S_{ij} = 5$ by ferromagnetic

exchange, leading to thermally accessible states of the form $|(S_{14} = 5, S_{23} = 5)S\rangle$. In the ground state, the pair spins, S_{14} and S_{23}, are coupled to $S = 0$ by antiferromagnetic exchange. The excited states occur in the order $S = 1, 2, ...$, and their exchange energies are described by the Hamiltonian in eq 6. The factor

$$H = {}^1/_2 J S_{14} \cdot S_{23} = {}^1/_4 J[S^2 - S_{14}^2 - S_{23}^2] \qquad (6)$$

one-half in the second term expresses the fact that two out of four possible interpair couplings are zero. The energies of eq 6 for $J = 728$ cm^{-1} are given by eq 5 if we substitute therein $J = 364$ cm^{-1} and $S_{13} = S_{24} = 5$. Thus, the energy spectra for eq 3 at the two extremes have a ground state with $S = 0$ and excited states with $S = 1$ and 2, lying at 364 and 1092 cm^{-1}, respectively, above the ground state. A similar pattern is found throughout the entire range of solutions. The states at the extremes are characterized by "good" quantum numbers, S_{14} and S_{23} at the left extreme, and by S_{13} and S_{24} at the right extreme. The quantum numbers S_{13} and S_{24} involve the local spins at the termini of the noninteracting diagonals which belong to different cubanoid moieties. S_{14} and S_{23} are the spins of either the cubanoid moieties or the coupled fragments, depending on whether one assigns J' to intracubanoid or intercubanoid interactions. Thus, only in the former case can the spins of the cubanoid moieties be considered good quantum numbers.

Although the points on the left branch (Figure 7, inset) are mathematical solutions to the fitting problem, they cannot be considered as acceptable physical solutions, because (i) Fe−S−Fe bridges have never been found to support ferromagnetic exchange coupling ($J' < 0$)[24] and (ii) values of J greater than 550 cm^{-1} are somewhat unrealistic. Both the magnitude and the antiferromagnetic sign of the solutions for J and J' on the right branch are better in line with the expectations. Thus, assuming that $J = J'$, the solution is 364(30) cm^{-1},[25] while by adopting for the *intracubanoid* coupling the value $J = 280$ cm^{-1} as obtained recently for a [2:2] site-differentiated cubane,[16] the correlation plot in Figure 7 yields $J' = 445(60)$ cm^{-1} for *intercubanoid* coupling.[25] More generally, if the *intracubanoid* coupling is assumed to be weaker than the *intercubanoid* coupling, the value for the latter coupling is found to be greater than 364(30) cm^{-1}.[24] The reverse ordering, $J_{intra} > J_{inter}$, although it cannot be excluded on the basis of the available data, is less likely because from it would result a considerably larger value for the intracubanoid coupling ($J_{intra} > 364(30)$ cm^{-1})[24] than was determined previously (280 cm^{-1}).[16] Hence, the intercubanoid coupling is most likely strong and, as a consequence, the spins of the cubanoid moieties cannot be assumed to be good quantum numbers. In this context, it is to be noted that just this very assumption has been made in a recent analysis of the spin states of the P^{OX} cluster in nitrogenase.[26] Although the present results do not support an approach based on "frozen" spin states for the cubanoid subunits, the following points of possible pertinence to its applicability are to be considered: first, the oxidation states of the iron atoms in P^{OX} have predominantly ferrous character, and, second, the linkage of the cubane moieties in the P cluster is provided by cysteinyl bridges. As our results are for a system with sulfide-bridged Fe(III) sites, the relative magnitude of intra- and intercubane exchange herein should differ from that in the P cluster.

Acknowledgment. This research was supported by NIH Grant GM 28856 at Harvard University and NSF Grant MCB 94-06224 at Carnegie Mellon University. We thank B. E. Segal for assistance.

Supporting Information Available: Crystallographic data for the compounds in Table 1, including tables of crystal and intensity collection data, positional and thermal parameters, and interatomic distances and angles, and magnetic susceptibility data for compound **6** are available (23 pages). Ordering information is given on any current masthead page.

IC980085T

(24) All rhomboidal $[Fe_2(\mu_2\text{-}S)_2]^{2+}$ units in synthetic compounds and proteins are antiferromagnetically coupled; see: (a) Gillum, W. O.; Frankel, R. B.; Foner, S.; Holm, R. H. *Inorg. Chem.* **1976**, *15*, 1095. (b) Sands, R. H.; Dunham, W. R. *Q. Rev. Biophys.* **1975**, *7*, 443. All three examples of the (nonlinear) $[Fe_2(\mu_2\text{-}S)]^{4+}$ unit are antiferromagnetically coupled: (c) Dorfman, J. R.; Girerd, J.-J.; Simhon, E. D.; Stack, T. D. P.; Holm, R. H. *Inorg. Chem.* **1984**, *23*, 4407. (d) Mukherjee, R. N.; Stack, T. D. P.; Holm, R. H. *J. Am. Chem. Soc.* **1988**, *110*, 1850.

(25) The number in parentheses is the estimated error associated with the subtraction of contributions for paramagnetic impurities, diamagnetism, and temperature-independent paramagnetism from the raw data (cf. ref 16).

(26) Mouesca, J. M.; Noodleman, L.; Case, D. A. *Inorg. Chem.* **1994**, *33*, 4819.